Naval Research Laboratory
Washington, DC 20375-5320

NRL/7330/MR—2024/1

Examining a Transport Pathway in the East Sea/Sea of Japan

CONRAD A. LUECKE

Physical Oceanographic Processes Section
Oceans Sciences Division

May 20, 2024

REPORT DOCUMENTATION PAGE

PLEASE DO NOT RETURN YOUR FORM TO THE ABOVE ORGANIZATION

1. REPORT DATE	2. REPORT TYPE	3. DATES COVERED	
20-05-2024	NRL Memorandum Report	START DATE 01/11/2022	END DATE 01/11/20223

4. TITLE AND SUBTITLE

Examining a Transport Pathway in the East Sea/Sea of Japan

5a. CONTRACT NUMBER	5b. GRANT NUMBER	5c. PROGRAM ELEMENT NUMBER
		NISE
5d. PROJECT NUMBER	**5e. TASK NUMBER**	**5f. WORK UNIT NUMBER**
		H21H

6. AUTHOR(S)

Conrad A. Luecke

7. PERFORMING ORGANIZATION / AFFILIATION NAME(S) AND ADDRESS(ES)

Naval Research Laboratory
4555 Overlook Ave SW
Washington, DC 20375-5320

8. PERFORMING ORGANIZATION REPORT NUMBER

NRL/7330/MR—2024/1

9. SPONSORING / MONITORING AGENCY NAME(S) AND ADDRESS(ES)	10. SPONSOR / MONITOR'S ACRONYM(S) NUMBER	11. SPONSOR / MONITOR'S REPORT NUMBER(S)
Naval Research Laboratory 4555 Overlook Ave SW Washington, DC 20375-5320	NRL-NISE	

12. DISTRIBUTION / AVAILABILITY STATEMENT

DISTRIBUTION STATEMENT A: Approved for public release; distribution is unlimited.

13. SUPPLEMENTAL NOTES

Karles Fellowship

14. ABSTRACT

The East/Japan Sea (JES) is a marginal sea surrounded by Korea, Russia, and Japan. The Tsushima Warm Current (TWC) is one of the major flows into the JES, entering through the Korea/Tsushima Strait. The TWC is known to split into three main branches in the southern part of the JES: the first and second branches that split South (nearshore branch) and North of Tsushima Island (offshore branch), respectively, and the East Korea Warm Current (EKWC), which hugs the Korean coast as it flows northward. Results from a December 2021 drifter release reveal a surface current flowing eastward along the southern margin of the Ulleung Basin in the southwestern JES, which suggests a more northern pathway connecting the EKWC with the nearshore branch of the TWC along the coast of Japan. Contemporary drifter trajectories within high-resolution ocean models reveal a consistent pattern. Dispersion estimates from the drifter release reveal nonlocal processes influence spreading at scales below 10km, and local processes dominate at larger scales, which is consistent with the regional internal Rossby radius. We present estimates of TWC branch transports using 24 years of geostrophic velocity derived from satellite altimetry. This analysis suggests that the along-shelf transport is significant to the regional flow. Time-averaged along-shelf transport accounts for approximately 16% of the total TWC transport of 2.6 Sverdrups (Sv), with a seasonal maximum of between 0.5 and 1 Sv occurring in July-August. The along-shelf transport also exhibits a greater degree of 30-60 day sub-seasonal variability than is observed in other TWC branches (offshore branch and EKWC). This variability is also confirmed in an 8-month long nearby moored velocity record. Relative vorticity derived from satellite altimetry shows little difference between upstream conditions during high and low transport. However, the presence the Ulleung Warm Eddy is observed during times of low along-shelf transport, which suggests that interactions between the TWC and eddies within the Ulleung Basin play an important role in branching variability.

15. SUBJECT TERMS

Physical Oceanography, Lagrangian Drifters, Tsushima Warm Current Branching, Japan/East Sea Dynamics

16. SECURITY CLASSIFICATION OF:			17. LIMITATION OF ABSTRACT	18. NUMBER OF PAGES
a. REPORT	b. ABSTRACT	c. THIS PAGE	SAR	40
U	U	U		

19a. NAME OF RESPONSIBLE PERSON	19b. PHONE NUMBER *(Include area code)*
Conrad A. Luecke	(288) 688-5251

This page intentionally left blank.

CONTENTS

LIST OF FIGURES

LIST OF TABLES

1. Executive Summary

The East/Japan Sea (JES) is a marginal sea surrounded by Korea, Russia, and Japan. The Tsushima Warm Current (TWC) is one of the major flows into the JES, entering through the Korea/Tsushima Strait. The TWC is known to split into three main branches in the southern part of the JES: the first and second branches that split South (nearshore branch) and North of Tsushima Island (offshore branch), respectively, and the East Korea Warm Current (EKWC), which hugs the Korean coast as it flows northward. Results from a December 2021 drifter release reveal a surface current flowing eastward along the southern margin of the Ulleung Basin in the southwestern JES, which suggests a more northern pathway connecting the EKWC with the nearshore branch of the TWC along the coast of Japan. Contemporary drifter trajectories within high-resolution ocean models reveal a consistent pattern. Dispersion estimates from the drifter release reveal nonlocal processes influence spreading at scales below 10km, and local processes dominate at larger scales, which is consistent with the regional internal Rossby radius. We present estimates of TWC branch transports using 24 years of geostrophic velocity derived from satellite altimetry. This analysis suggests that the along-shelf transport is significant to the regional flow. Time-averaged along-shelf transport accounts for approximately 16% of the total TWC transport of 2.6 Sverdrups (Sv), with a seasonal maximum of between 0.5 and 1 Sv occurring in July-August. The along-shelf transport also exhibits a greater degree of 30-60 day sub-seasonal variability than is observed in other TWC branches (offshore branch and EKWC). This variability is also confirmed in an 8-month long nearby moored velocity record. Relative vorticity derived from satellite altimetry shows little difference between upstream conditions during high and low transport. However, the presence the Ulleung Warm Eddy is observed during times of low along-shelf transport, which suggests that interactions between the TWC and eddies within the Ulleung Basin play an important role in branching variability.

This report represents the results of research supported by the Jerome and Isabella Karle Distinguished Scholar Fellowship from the U.S. Naval Research Laboratory, and is organized as follows: In section 2, we present an overview of the current state of understanding of current branching and transport in the JES, along with a motivation for the work done in this study. In section 3, we describe the drifter data in which a novel along-shelf transport pathway is noted. We then examine drifter dispersion and make estimates of local eddy diffusivity in the JES. We then outline the methodology used for estimates of drifter dispersion rates and make comparisons to model output. Section 4 details the moored dataset collected as part of the MJES field campaign. We then describe some of the low frequency flow characteristics observed at the mooring and compare surface velocities at the mooring with geostrophic currents from satellite altimetry. Additionally, we explore the role of wind-driven Ekman flow. Lastly, in section 5, we extend the analysis of the branching behavior of the TWC to a 24-year dataset of geostrophic velocities derived from sea surface height. We then compare our transports with estimates made in previous literature, in regions where this is possible. We then present an analysis of the variability of the shelf branch transport. Furthermore, we examine 24 years of relative vorticity to explore possible dynamic explanations for branching behavior. Finally, a discussion of the results and conclusions are given in section 6.

This page intentionally left blank.

2. Introduction

The Sea of Japan/East Sea (JES), a partially enclosed marginal sea, is bordered by the Korean peninsula and continental Eurasia on the West, and the Japanese archipelago to the east. It is connected to the Pacific Ocean, the East China Sea, and the Sea of Okhotsk by four shallow straits: the Korea/Tsushima, Tsugaru, Soya, and Mamiya Straits. The Tsushima Warm Current (TWC) is relatively warm current originating from the Kuroshio Current that enters the JES through the Korea/Tsushima Straight (KTS). The TWC plays a significant role in transporting heat and nutrients from the subtropical Pacific Ocean to the JES, and ultimately influences the climate and ecosystems of the region.

Previous research has identified the TWC system as comprising three distinct current branches, as has been outlined in numerous studies (Suda and Hidaka in 1932, Kawabe 1982, Lie 1984, Preller and Hogan 1998, Cho and Kim 2000, Yabe et al. 2021, to name a few). As the TWC approaches the Korean Peninsula, it begins to split into several smaller branches. The first branch occurs as a portion of the current splits south of Tsushima Island and continues along the coast of Japan. The current that travels north of Tsushima island then splits again, with a second branch moving eastward into the interior of the Ulleung Basin. The remaining third branch travels north along the Korean coast. Although there is some degree of variability in the naming conventions for these respective branches, it is generally understood that the first branch is also known as the nearshore branch, the second branch is referred to as the offshore branch, and the third branch is referred to as the East Korea Warm Current (EKWC), which is the naming convention that we have chosen to adopt for this report.

The nearshore branch is understood to have a source on the eastern channel (Japanese side) of the KTS, traveling along the Japanese coastline, as was documented by Kawabe in 1982. The offshore branch and the East Korean Warm Current originate from the western channel of the same strait. The former travels westward into the Ulleung Basin, where it is confined by the slope along Japan's main island, while the latter flows northward along the Korean Peninsula and bifurcates again downstream. In some instances, the offshore branch has been observed following a more southward trajectory than typically described in previous literature, flowing along the southern edge of the Ulleung Basin shelf break. This branching was consistent with the drifter tracks reported in this work, and also noted in Lee and Niiler (2010), although the latter classify this branching pattern as atypical. It is also noteworthy that Lee and Niiler (2010) did not observe this branching during the winter months, which somewhat contradicts the 2021 drifter observations we present in this report.

Numerous studies have aimed to further define and characterize the branching pathways of the TWC. Hydrographic, satellite-tracked drifters, and satellite altimetry data have been utilized to observe the presence of the three main branches and their seasonal variability in the JES (Kawabe, 1982; Kato 1994; Lee and Niiler, 2010; Ito et al., 2014). Morimoto and Yanagi (2001) presented monthly mean current data based on altimetry, while Hase et al. (1999) inferred variability in the nearshore branch using temperature at 100 m depth along

Manuscript approved May 13, 2024.

with tracks of surface drifters. While most literature agrees on the general structure of TWC branching, ongoing discussions persist regarding the behavior of an along-shelf or offshore branch. Kawabe (1982) notes a pronounced seasonality in the appearance of the offshore branch, while Morimoto and Yanagi (2001) argue that the branch exhibits minimal seasonal fluctuations. Both the nearshore branch and the EKWC are known to persist throughout the year (Kawabe, 1982a; Hase et al., 1999), although some seasonal variability has been noted (Yabe et al. 2021).

The relationship between the meandering pathway of the TWC and the three branches remains unclear. Lee and Niiler (2010) suggest that the TWC meanders as a singular pathway, mostly without bifurcations into branches, and that the significant variations in the circulation pattern of the Ulleung Basin are governed by these meanders, which are controlled by inflow conditions through the KTS. Lee and Niiler (2010) also find that the circulation patterns downstream of the KTS were determined by the relative vorticity of the flow within the strait. If the flow had large negative vorticity, it resulted in the flow pattern we later describe in this report as the shelf branch. Additional factors contributing to the complexity of the TWC system include the intensity of eddy activity, leading to multi-scale meanders and bifurcations (e.g., Isoda 1994; Hirose and Ostrovskii 2000; Watanabe et al. 2009). While the exact role played by inflow conditions such as vorticity through the KTS is unknown, it is evident that a major factor influencing TWC system is the volume transport entering the sea through the KTS, and the subsequent volume transports of each branch or circulation pattern. The goal of this study is to examine the importance of these factors.

In this report, we focus on the branching characteristics and behavior driven by the TWC, particularly with respect to the along-shelf branch behavior. As far as we are aware, there has been no detailed analysis of the volume transport attributed to the shelf branching behavior. Motivated by this, we present a detailed analysis of surface drifter tracks from a 2021 drifter experiment collected as part of a collaborative effort between several South Korean institutions and the U.S. Naval Research Laboratory (NRL) project, “Mixing in the Japan/East Sea (MJES)”. This study utilizes drifter tracks from an 18-drifter release, high resolution model output, and 24 years of satellite-based altimetric data to enhance the characterization of the northern branch of the TWC. Drifter tracks are compared with contemporary tracks from U.S. Navy operational models run by NRL, and we then extend our analysis to 24 years of satellite data.

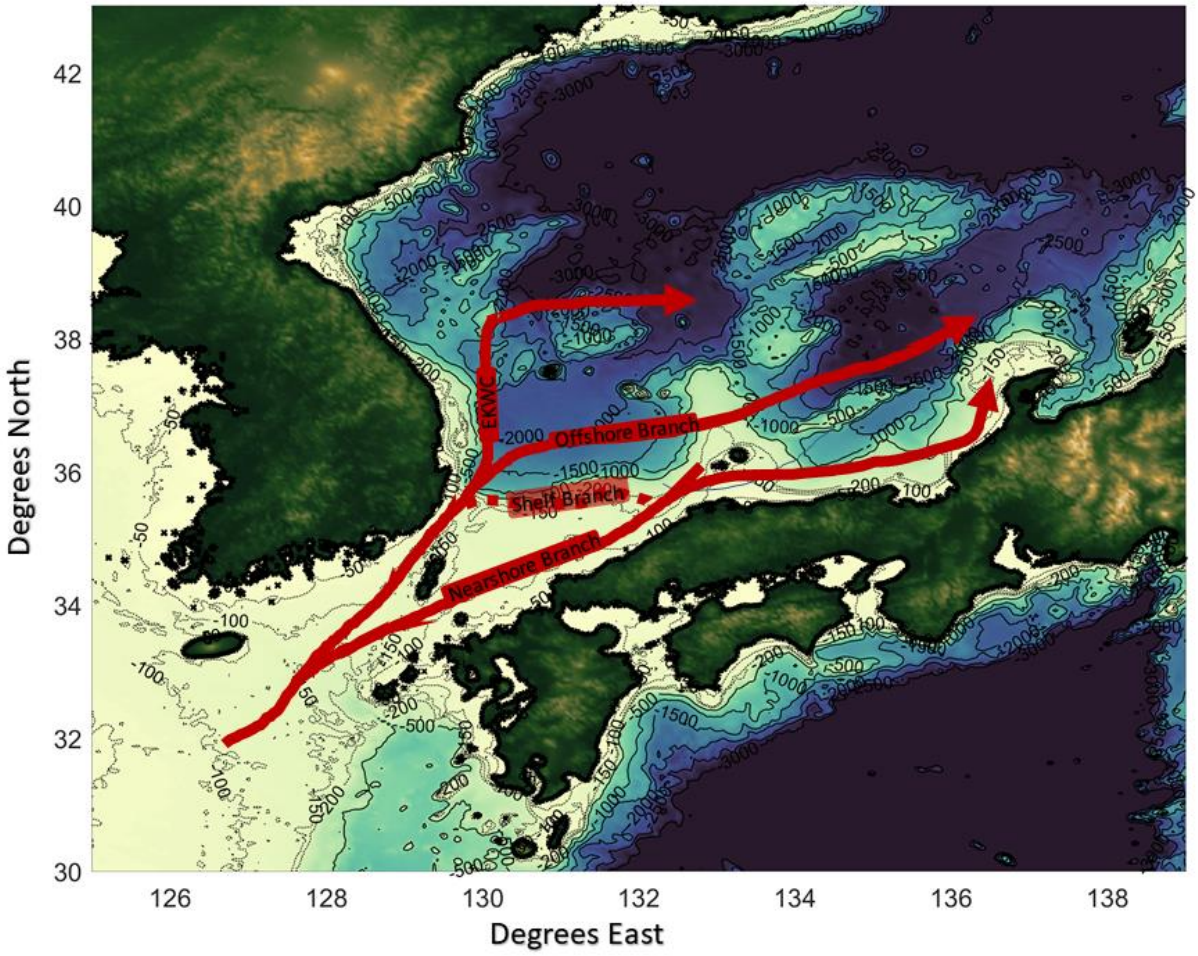

Figure 1. Cartoon schematic of the Tsushima Warm Current (TWC) and the branch locations (Following Preller and Hogan 1998). The Nearshore Branch (first), Offshore Branch (second), and East Korean Warm Current (third) branches are shown as solid red lines. The broken red line depicts the intermittent transport pathway or "along-shelf branch" that is the subject of this study.

3. Drifter Release Experiment

Lagrangian drifters are an important tool for quantifying ocean circulation and currents, as well as increasing our understanding of how tracers (biological, physical, anthropogenic) are dispersed. As part of the December 2021 component of the MJES field experiment, 18 drifters were released in the southern JES. The drifter tracks reveal a surface current flowing eastward along the southern margin of the Ulleung Basin in the southwestern JES. Here we present an analysis of the drifter dispersion, along with comparisons to model output.

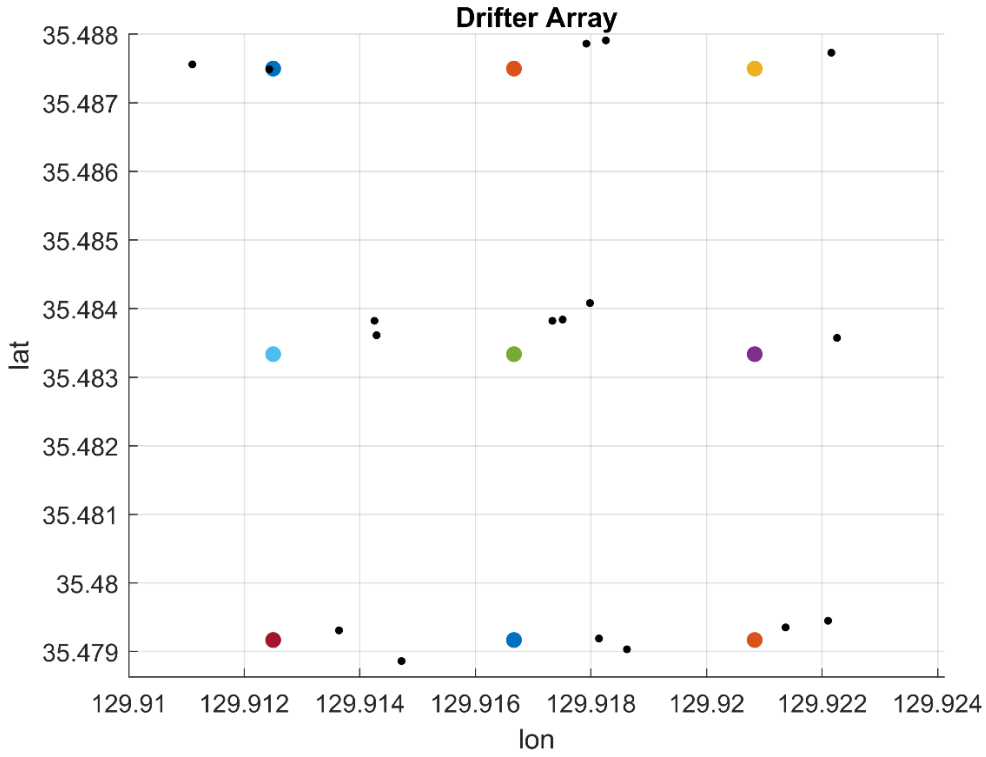

Figure 2. Map of drifter release pattern. Drifters were released in a 3x3 grid/array spanning about 1km. Clusters of 2-3 drifters were released at most points in the grid. 18 drifters yielded 153 "pairs" that can be used to calculate dispersion

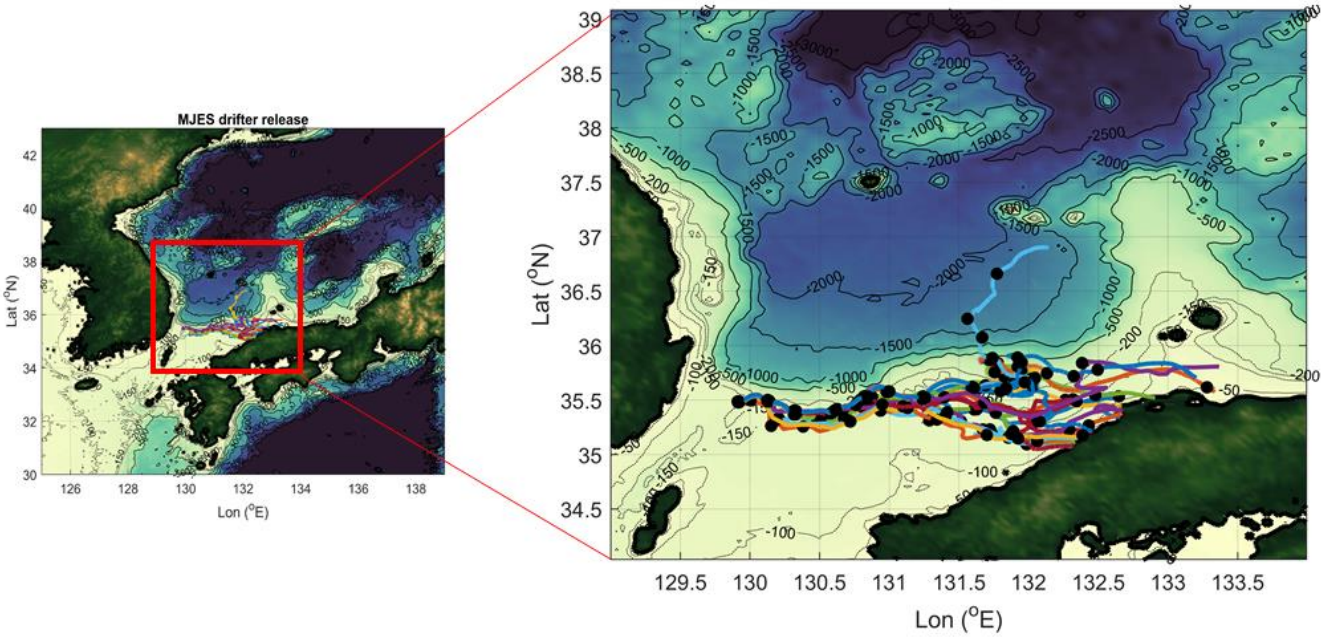

Figure 3. Left Panel: map of study area showing drifter release. Right panel: expanded view of individual drifter tracks. Black dots represent 24 hour intervals of drifter movement. The depth is shown with contours in each plot.

3.1 Drifter dispersion and eddy diffusivity estimates

Drifters were released in a 3x3 pattern array spanning about 1km. Clusters of 2-3 drifters were released at most points in the grid. The ten-minute sampling of the drifter location allowed for the examination of small-scale/high-frequency processes. 18 drifters yielded 153 "pairs" that can be used to calculate dispersion: Clusters of 2-3 drifters were released at most points in the grid. 18 drifters yielded 153 "pairs" that can be used to calculate dispersion:

$$D^2(t) = \frac{1}{N}\sum_{i\neq j}^{N}\left\|x_i(t) - x_j(t)\right\|^2 \qquad (1)$$

Drifter dispersion as a function of time can be seen Figure 4. Individual tracks show large variability, sometimes with low separation and convergence amongst drifter pairs early in the timeseries. When averaged, drifter dispersion is initially high, possibly following exponential growth consistent with non-local dispersion. Both dispersion and diffusivity are calculated using the methods outlined in Drinkwater and Loder 2001. From 0 to 1 day and at separation scales up to 10 km, the relative dispersion increases exponentially in time with a growth rate of 6, which corresponds to an e-folding time of ~0.17 days. In this phase, the observations are consistent with relative dispersion dominated by processes much larger than the drifter separation, which is an indicator of a nonlocal dispersion regime. After this initial phase and at scales larger than 10 km, the relative dispersion briefly flattens out, and then transitions to a power-law dependency in the scaling of:

$$D^2 \propto t^n \qquad (2)$$

For times larger than 2 days, the dispersion of the estimated slope follows the theoretical prediction by Richardson and scales as t^3. The spreading of the drifters in this regime is mainly influenced by current characteristics of scales similar to the drifter separation, which is consistent with the basin scale internal Rossby radius of ~10-20km. Diffusivity estimates can be made by regressing D^2 over the time of drifter deployment. Because the dispersion characteristics change time, there is some variability to estimates of diffusivity, depending on the time frame being examined. On bulk, over all drifters, and during the December deployment, the diffusivity estimates range from 1–5 $\times 10^3$ m^2 s^{-1} which are consistent with previous findings such as Toba et al 1984, who estimated a diffusivity of 5 $\times$ 10^3 m^2 s^{-1} in the southern JES. Similarly, Oh et al 2000 found the diffusivity in the JES to be between 1.7 $\times 10^3$ m^2 s^{-1} and 5.2 $\times 10^3$ m^2 s^{-1} over timescales of 0.7–1.7 days, and length scales of 10–25 km, which are comparable with the length scales sampled by our drifter release.

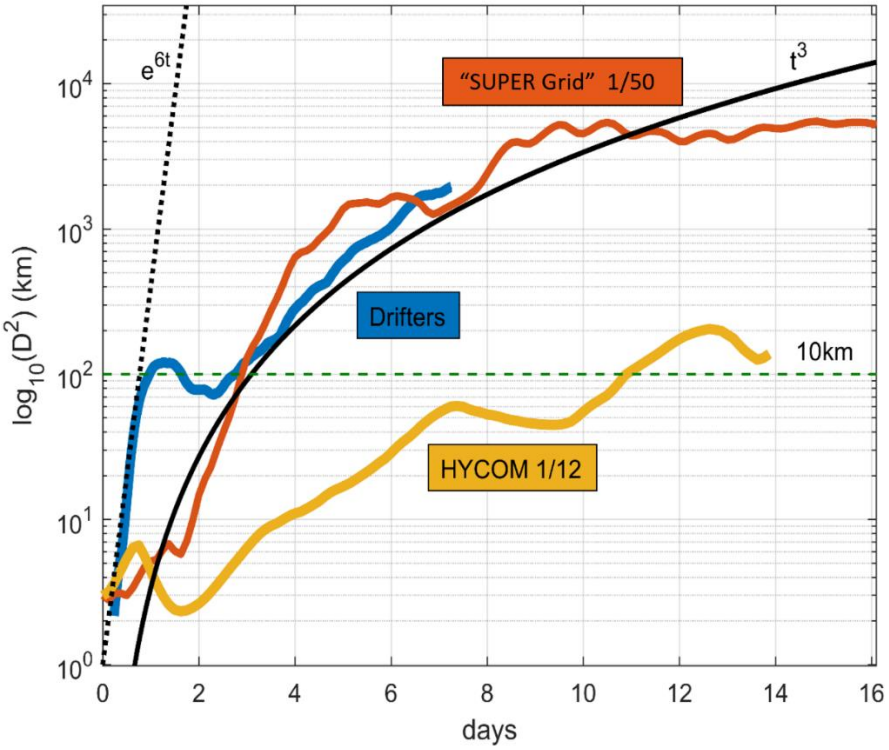

Figure 4. Dispersion vs. time (D^2) for drifter release experiment in observations, HYCOM 1/12 degree and COAMPS/HYCOM "SUPER-GRID" runs.

3.2 Drifter comparisons with model output

In the following, we use high-resolution model output to examine the surface currents during the observational period. Model drifters are released from the same location and advected with the surface currents in two different NRL developed models. The first model comparison utilized the HYbrid Coordinate Ocean Model (HYCOM) (Chassignet et al., 2009) and will be herein referred to as HYCOM12. NRL operates the Global Operational Forecasting System (GOFS), which is a HYCOM-CICE coupled model configured globally at 1/12° equatorial horizontal resolution and with a 41-layer hybrid vertical structure (Metzger et al. 2014). The model is forced by 3-hourly atmospheric fluxes derived from the Navy Global Environmental Model (NAVGEM; Hogan et al. 2014) and assimilates observations via 3D-variational analysis once daily at 1200 UTC. The model smoothly adjusts the subsurface via dynamical balance and mixing through the water column. The model turbulence closure is parameterized with a K-profile parameterization scheme for vertical mixing (Large et al. 1994). The model incorporates a realistic bathymetry derived from the 30-arc-s GEBCO-2014 data (Weatherall et al. 2015) with the coastline set at the 5-m isobath. While similar Global HYCOM predecessors have been running since the 1990s, GOFS has been running in this configuration since 2018. Similar

HYCOM predecessors are known to possess a realistic global mesoscale eddy field that has been extensively validated against observations (Luecke et al. 2017).

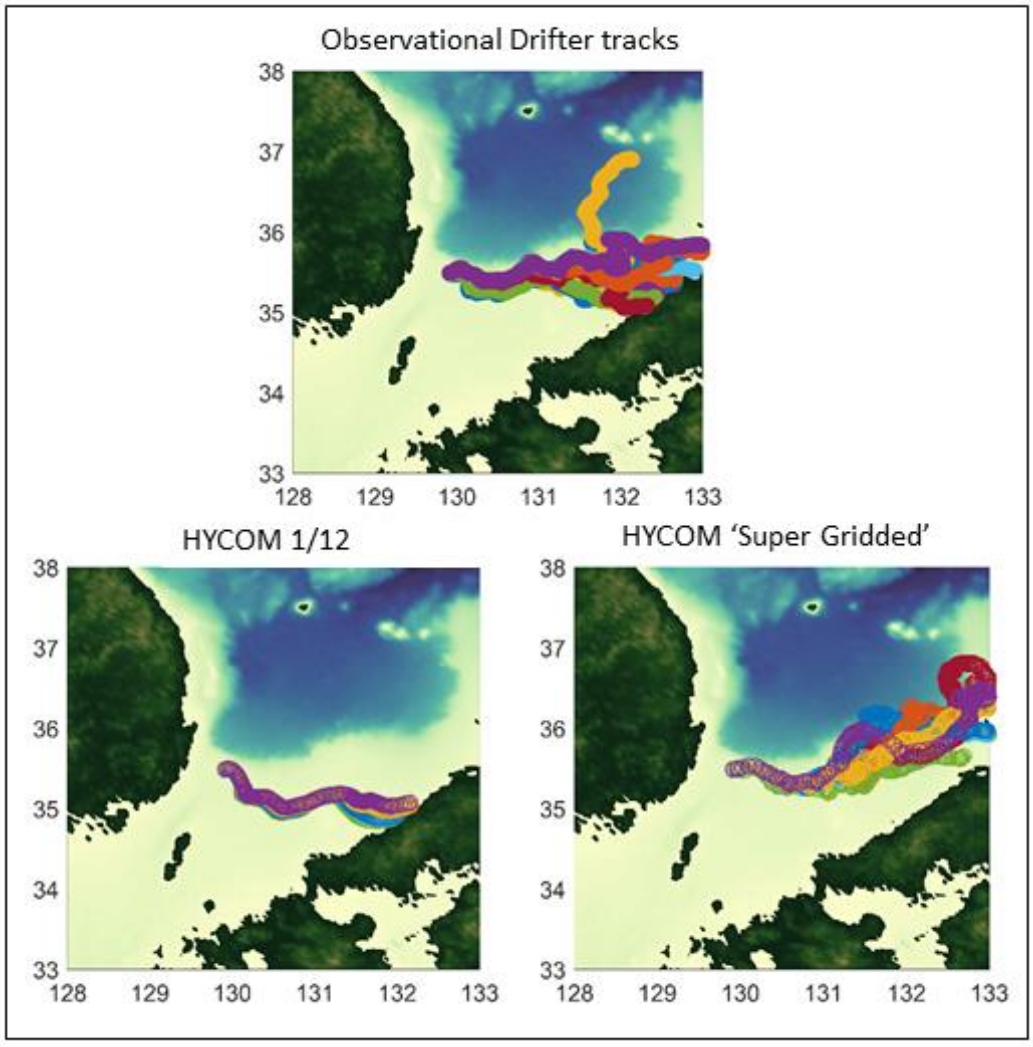

Figure 5. Maps of drifter release experiment in observations, HYCOM 1/12 degree and COAMPS/HYCOM "SUPER-GRID" runs.

A second model run compared is an objectively mapped blend of the Coupled Ocean–Atmosphere Mesoscale Prediction System (COAMPS) and HYCOM12 over the study domain. The COAMPS regional run used in this study includes an atmospheric, ocean, and wave models that are fully coupled, covering the JES. The COAMPS model uses 60 vertical levels for both the atmosphere and the ocean. Vertical mixing is computed using the 2.5-level turbulence closure scheme by Mellor and Yamada (1982), modified to include contributions from Stokes drift and Langmuir circulations (Kantha and Clayson, 2004). The COAMPS has horizontal resolutions of 2 km in the ocean and 6 km in the atmosphere and like the HYCOM12 run utilizes the 30-arc-s GEBCO-2014 bathymetry. The ocean model is covered by a spherical grid with a resolution of

1/54° on a 1600 by 1320 grid with a time step of 5s. The ocean model is initialized and its boundaries are forced every 6 hours by output from the 1/12° global HYCOM. The ocean model includes evaporative and precipitate fluxes, and eight semidiurnal and diurnal tidal forcing components. Monthly climatological discharges of river outputs are included in the ocean model. This model run will be referred to as COAMPS/HYCOM SG. In both models, drifters were released in the locations described in Section 3.1, and advected forward in time for the duration of the drifter experiment.

While both model runs have some characteristics that mirror the path of the drifter tracks, there are several noteworthy differences, which can be seen in the modeled drifter tracks shown in Figure 5. In the case of the 1/12° HYCOM, the drifters travel eastward but follow a somewhat more southerly trajectory. In the SG run, the drifters follow a track that is closer to observed paths, apart from one drifter which escapes northward into the basin in the observations and does not in the model run. Another visible difference between the two model runs is that in the 1/12° HYCOM run, the drifters exhibit visually less dispersion. This is confirmed when dispersion is calculated within each model run. Drifter dispersion is calculated in a consistent manner in both model analysis and in observations. Dispersion vs. time curves for both model runs are shown in Figure 4. There are some differences in dispersion between models and observations at scales smaller than 10 km. In the COAMPS/HYCOM SG run, the drifters display more realistic dispersion characteristics; however, in both runs, the bulk drifter tracks follow a similar trajectory to the observations.

3.3 High-Frequency Drifter motion: Lagrangian wavelet analysis

Near-inertial, diurnal, and semi-diurnal tides are found to contribute to drifter motion. Velocity spectra from the drifters (Figure 6) show diurnal and semi-diurnal tides, and exhibit a transition from an f^{-2} super-tidal slope to a whiter spectrum at periods less than two hours. Drifters exhibit intermittent high-frequency motions. Although these motions seem linked to the passage of an atmospheric front, further work is needed to explain them. Possible explanations for these motions include nonlinear down-scaling of near-inertial motions interacting with the mean flow and eddy field, wind/wave (Langmuir) driven small-scale turbulence, Ekman layer adjustment process (spin up/down of near inertial motions). Work is also ongoing to determine if cycloid fits to translated vortical drifter motion provides an explanation for the observed high-frequency signals seen in the drifter tracks.

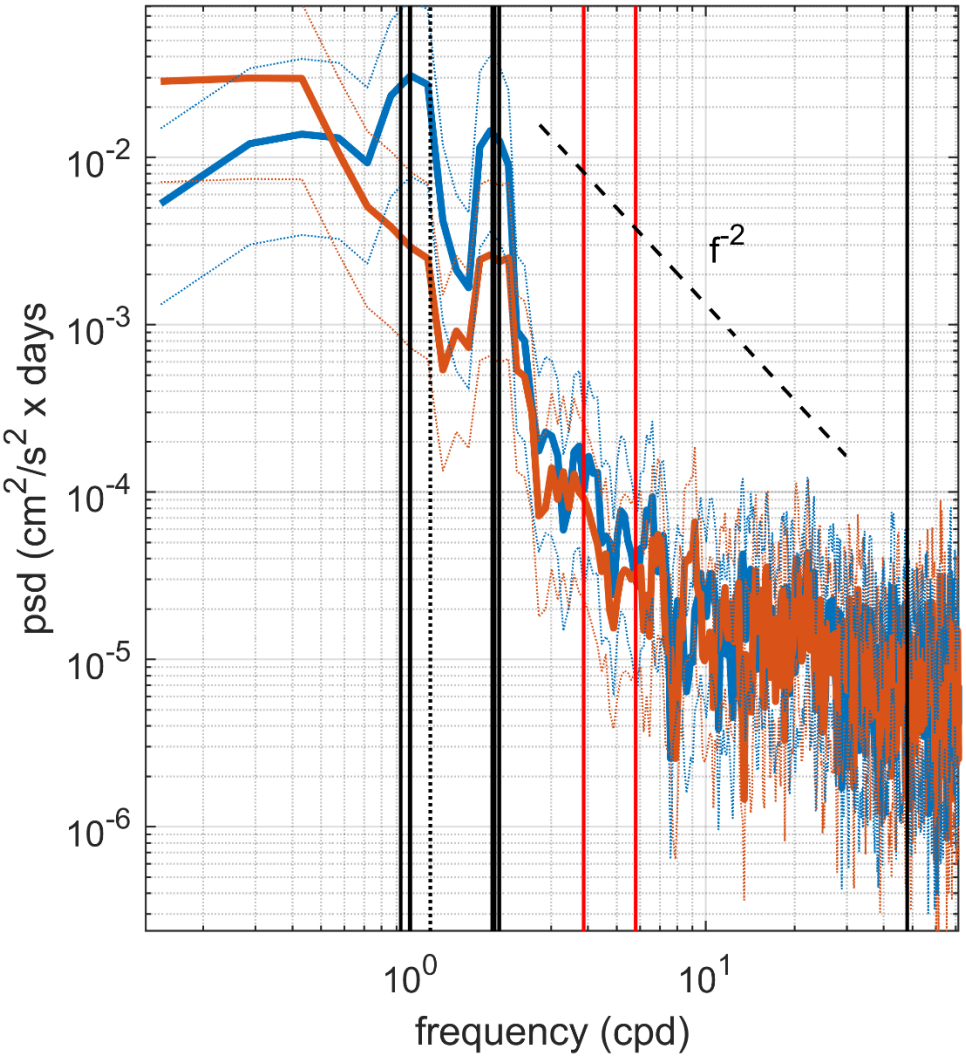

Figure 6. Rotary spectrum from a drifter exhibiting a transition from an f-2 super-tidal slope to a whiter spectrum at periods less than two hours. The vertical black lines (from left to right) indicate diurnal, (K_1, O_1), inertial, and semidiurnal (M_2, S_2) periods, and the red lines show the first and second harmonic of the semidiurnal tide.

One noteworthy feature of the drifter experiment was that the drifters exhibited intermittent super tidal variability in their velocity over the course of the deployment. To further illustrate variability over time, a continuous wavelet transforms (Torrence and Compo, 1998, Lilly, 2021) was performed for drifter velocity. Figure 7 shows (a) the U and V components of velocity for a single drifter over the course of deployment. An example rotary wavelet spectrum of Lagrangian velocity is shown in Figure 7 (b) and is shown again with more resolution at high frequency (c). Wavelet spectrum of velocity are proportional to the square of

velocity, and thus can be equated to kinetic energy (KE). Examination of the drifter KE spectra reveals a number of features: energy in the diurnal and semi-diurnal tidal bands, more clockwise energy in both the semi-diurnal band and diurnal band. This is both consistent with the tidal ellipses presented in Teague et al., 2001 and Book et al., 2004, as well as with wind generated near inertial oscillations in the northern hemisphere. Many drifters exhibit intermittent high-frequency motions with periods ranging from 1- 3 hours. These periods appear to coincide with large injections of energy into the inertial band (*f*). At this time, there is strong synoptic scale weather forcing as can be seen by the passage of a northerly atmospheric front in the ECMWF ERA5 reanalysis output (https://cds.climate.copernicus.eu/) wind (Figure 7d). Also at this time, local high-frequency KE and turbulent momentum flux (<u'v'>) (Figure 7e) appear to be linked abrupt changes in the wind field rather than the overall magnitude. During the wind event marked in the box, increased KE in the near-inertial band and at higher frequencies occurs during the passage of a northerly front.

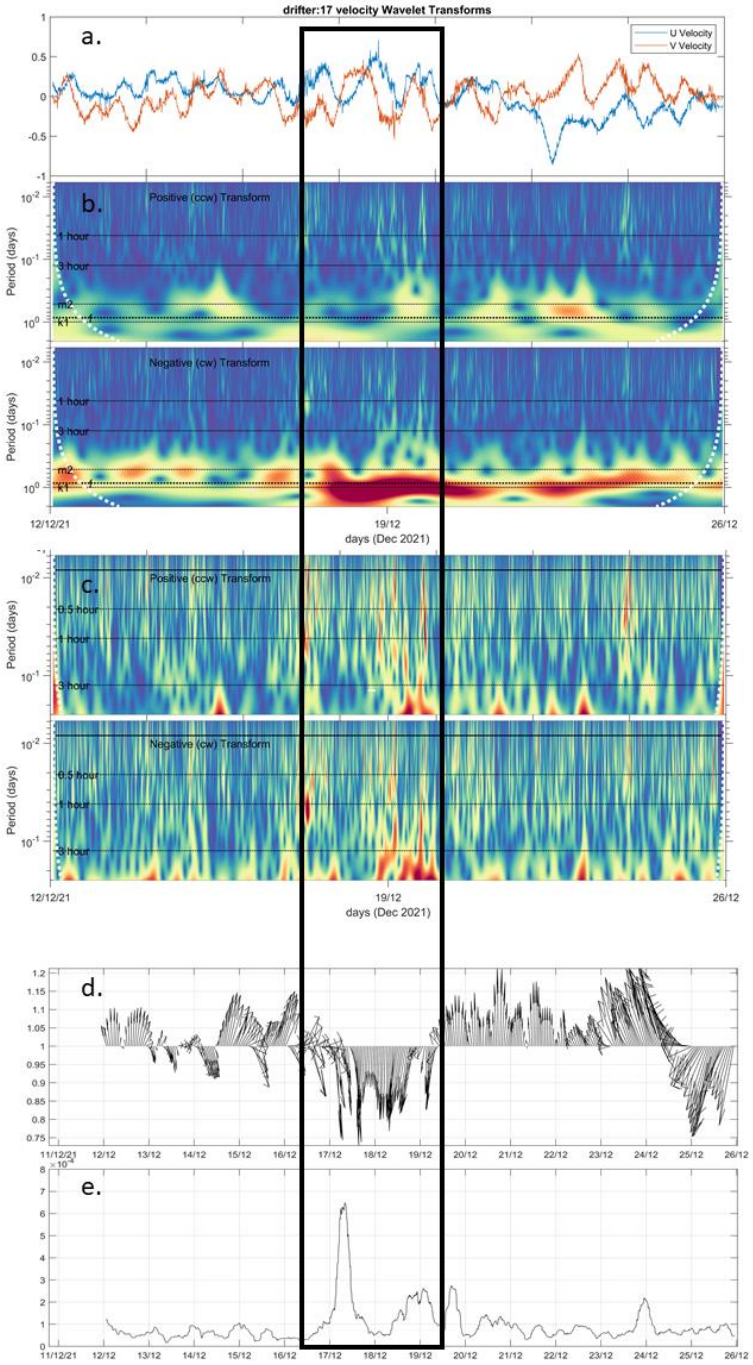

Figure 7. starting from top panel. A) U and V components of along path drifter velocity. B) positive and negative rotary wavelet transform of along track drifter velocity. C) same as B) but with highlight on high-frequency resolution. D) local wind forcing from ECMWF ERA5. E) eddy/turbulent momentum flux (<u'v'>) calculated using high-frequency drifter motions.

4. Mooring A3 Overview

As a component of the MJES campaign, a subsurface mooring was deployed in the JES from December 2021 to August 2022. The mooring (henceforth referred to as A3) was positioned on the southern shelf break of the Ulleung Basin in the southwestern JES at 35.69 degrees North and 130.16 degrees East, in a water depth of 910m. The A3 mooring was designed to collect both current and hydrographic data. However, the shallowest instrument was positioned at a depth of 400 m to avoid entanglement with fishing equipment, which is common in the region. Horizontal currents were measured using two 75-kHz acoustic Doppler current profilers (ADCPs), one positioned upward for the upper water column, and another 75-kHz ADCP to extend coverage to near the bottom. ADCP and other instrument locations and details for A3 can be found in Table 1 and the position of the mooring is shown in Figure 12. The ADCPs provided high quality velocity data throughout the water column; however, some parts of the upper-water column velocity data and near bottom records were excluded for low signal correlation. For the current data presented in this report, hourly velocity data was interpolated to an 8-m grid between the surface and the seafloor at 910m.

Instrument	Approximate Depth (M)	Variables Collected	Sampling Rate
ADCP WH75kHz	405	U,V (upward)	30 min
ADCP WH75kHz	409	U,V (downward))	30 min
SBE37	414	T,C,P	1 min
SBE39	440	T,P	1 min
SBE56	497	T	10 sec
SBE37	533	T,C,P	1 min
SBE56	559	T	10 sec
SBE37	596	T,C,P	1 min
SBE56	621	T	10 sec
SBE37	658	T,C,P	1 min
SBE56	683	T	10 sec
SBE56	745	T	10 sec
SBE37	784	T,C,P	1 min
SBE56	807	T	10 sec
SBE56	869	T	10 sec
SBE56	903	T	10 sec
SBE37	908	T,C,P	1 min

Table 1. List of instrument type, locations, and sampling rates for mooring A3.

Data was linearly interpolated between the instruments. A combination of instruments were used to measure temperature (T), conductivity (C), and pressure (P). SBE37 (T, C, P),

SBE39 (T, P), and SBE56 (T) sensors were installed between the top of the moorings and a depth of 908 m. Table 1 gives specific details about the sampling configurations and depths of these instruments.

4.1 Low Frequency Flow Characteristics at A3

Here we examine some of the low-frequency flow characteristics observed during the deployment of A3. Figure 8 shows 3-day low-passed U (top panel) and V velocity (middle), and temperature (bottom panel) at mooring A3 for the duration of mooring deployment. During the deployment, the mooring exhibits a host of strong dynamical features. Throughout the deployment the flow appears to be characterized by a two-layer system, with the first layer extending to about 200m, and the second layer extending from between 100-200m to the bottom.

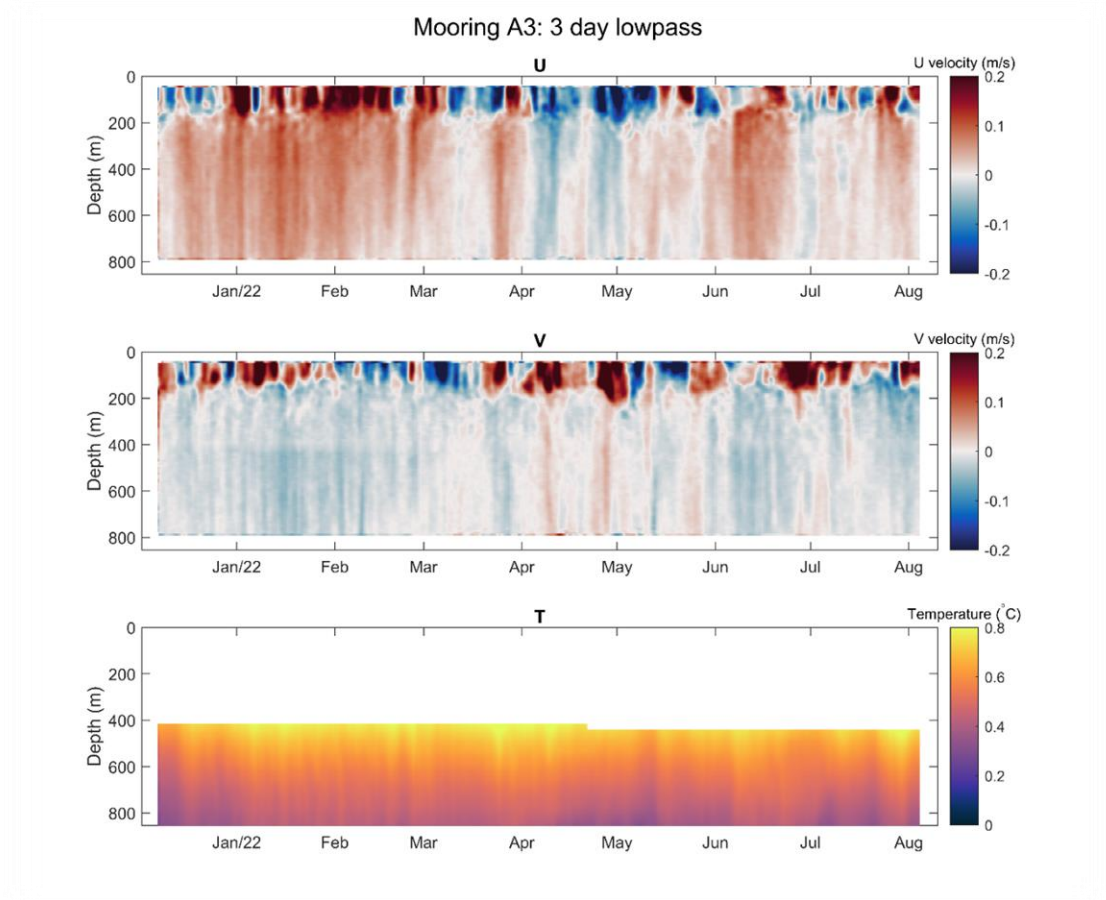

Figure 8. 3 day low-passed meridional (top) and zonal (middle) velocities, and temperature (bottom) at mooring site A3 for the duration of the deployment.

One characteristic feature of the upper layer is the presence of low-frequency flow reversals. These reversals occur on timescales of 20-40 days, and are consistent with the spatial/temporal scales of Rossby waves and eddies. The passage of these eddies/Rossby waves appears as a vertical banding in the meridional and zonal components of velocity.

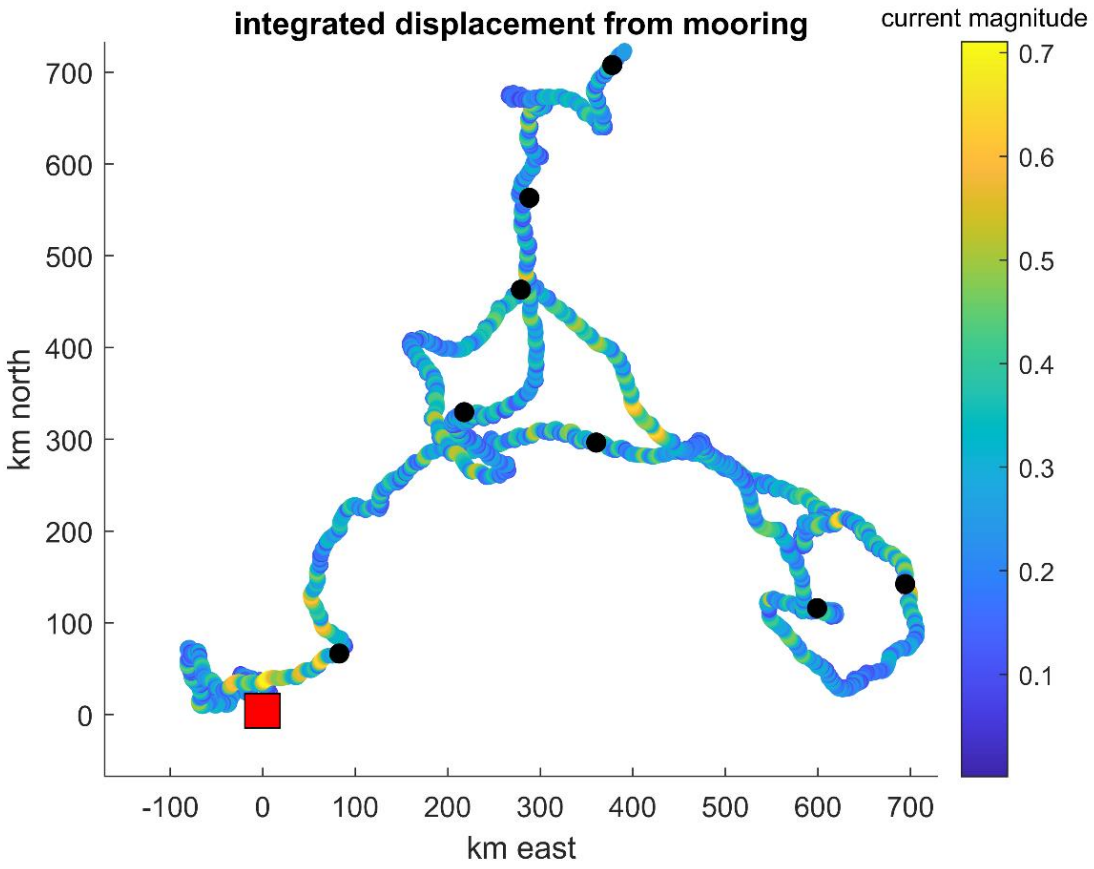

Figure 9. Progressive vector diagrams (PVDs) using depth-averaged velocities (0 to 200 m) are plotted on a spatial grid for mooring A3 in order to illustrate the current flow over the deployment period. 1-month intervals are represented as black dots along the PVD line.

Progressive vector diagrams (PVDs) using depth-averaged velocities (0 to 200 m) are plotted on a spatial grid for mooring A3 in order to illustrate the current flow over the deployment period (Fig. 8). The progressive vector diagram estimates the Lagrangian projection of the currents using ADCP Eulerian measurements at the mooring site. This shows how a water parcel would move if the current were the uniform along the track. The PVD highlights the long-term flow characteristics during the deployment and show the broad transport directions at that location within the JES. The PVD originates at the mooring location, marked by a red square. The directional variability and looping of the PVDs indicates some eddy variability throughout the course of the measurement period. Black dots along the track mark

one-month intervals during the mooring deployment. The PVD indicates that the cumulative flows at the A3 mooring site JES are to the northeast, and are toward the northeast throughout the upper 500 m.

4.2 Mooring Comparisons with Altimetry

In this section, we present the results of comparing surface currents observed at mooring site A3 with geostrophic currents calculated from altimetry data. The analysis aims to examine the agreement between low-frequency surface currents and altimetry-based estimates used to estimate transports in later sections, while exploring significant departures observed at higher frequencies.

Surface currents at mooring A3 are compared with geostrophic currents calculated from altimetry at the same time. While the low-frequency surface currents observed generally agree with the altimetry-based estimates, there are significant departures of on the order of 0.2 m/s from the low frequency signals occurring at periods less than 30 days. To discern the influence of wind-driven surface currents, we calculate currents resulting from Ekman transport, utilizing ECMWF ERA5 wind stress data during the mooring deployment period. Figure 10 illustrates the U and V components of velocity from mooring observations, geostrophic velocities derived from satellite altimetry, and the combined effect of geostrophic currents and ECMWF wind-driven Ekman currents. Although the addition of wind driven surface flow appears to add a similar characteristic of high-frequency variability as is observed at the mooring site, it is not clear that the signals are well correlated. Further examination of ERA5 Ekman transports confirms that the near surface Ekman transports do not play a large role in the regional transport examined within this study.

These findings underscore the complexity of surface current dynamics, highlighting the need for a nuanced understanding of the interplay between low-frequency signals, wind-driven currents, and their implications for regional transport. The observed departures and lack of clear correlation with wind-driven currents emphasize the multifaceted nature of oceanic processes, warranting further exploration and refinement of current models.

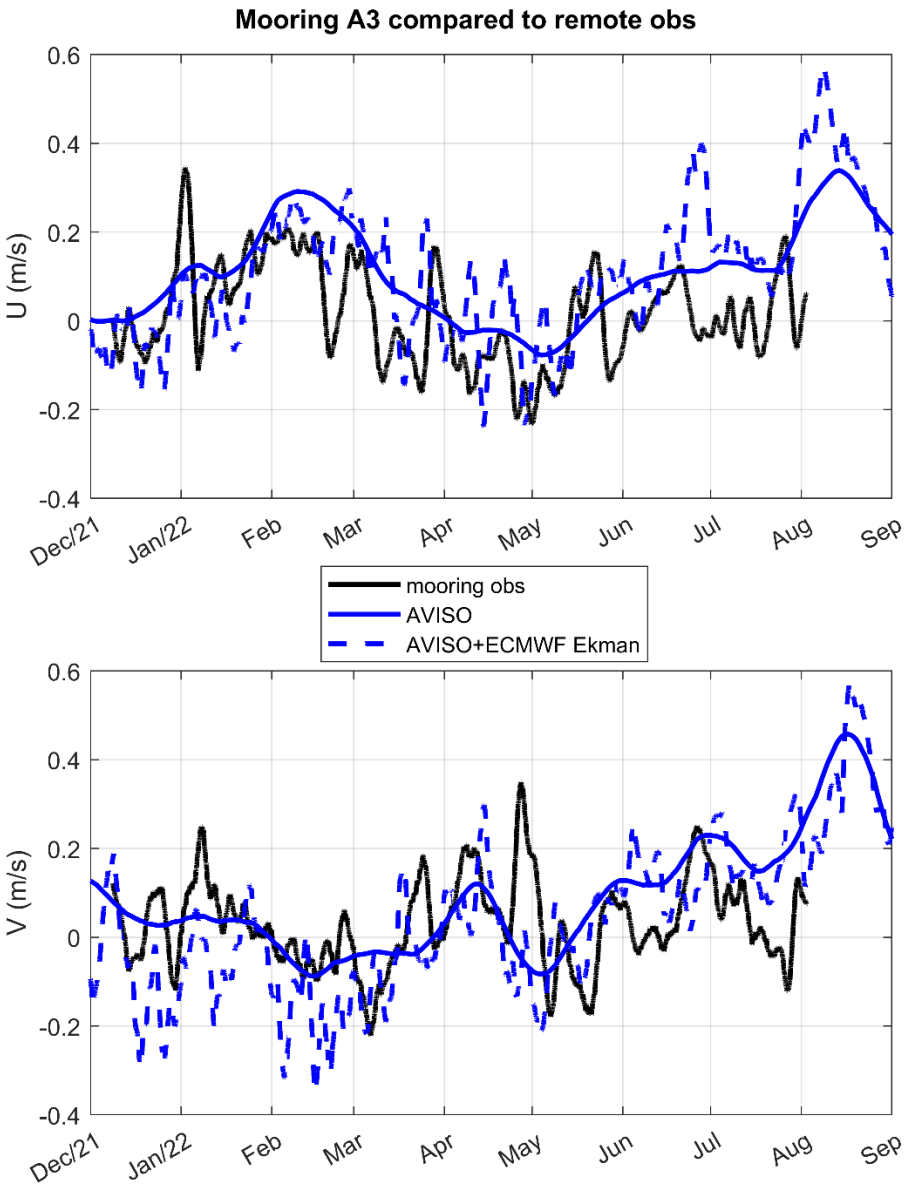

Figure 10. 10 day low-passed density and currents at A3 compared with geostrophic surface velocity (m/s) calculated using ERA5 ECMWF wind-stress reanalysis output

5. Transport Estimates from Altimetry

While the drifter experiment presented in Section 3 provides insight into the branching behavior of the TWC over the course of a relatively short time, and the mooring deployment described in section 4 provides some insight into the low-frequency variability of the currents in region, we extend our analysis of TWC branching to examine 24 years of remote sensing data.

This allows us to further constrain the annual and inter-annual variability of TWC branching as well as to estimate individual transports between different TWC branches. We utilize a satellite-based altimeter dataset titled "Global Ocean Gridded L4 Sea Surface Heights and Derived Variables Reprocessed," processed and distributed by the Copernicus Marine Environment Monitoring Service (CMEMS). CMEMS incorporates absolute dynamic topography and geostrophic velocity from various scientific missions such as TOPEX-Poseidon and Jason 1–3. The CMEMS dataset is processed daily with 0.25° resolution. The analysis presented in this report focuses on data covering the period from January 1998 through December 2022. Geostrophic currents averaged monthly for the duration of this time period in the JES are shown in Figure 11. The seasonal cycle of TWC and EKWC strength can clearly be seen, with high flow appearing in the summer and fall, followed by a more quiescent period in the winter/spring. Additionally, some effects of other prominent features such as the Dok Cold Eddy (DCE) Mitchell et al. (2005) and the Ulleung Warm Eddy (UWE) are present. However, the nature of the long-term averaging smears these signals which inherently contain eddy variability.

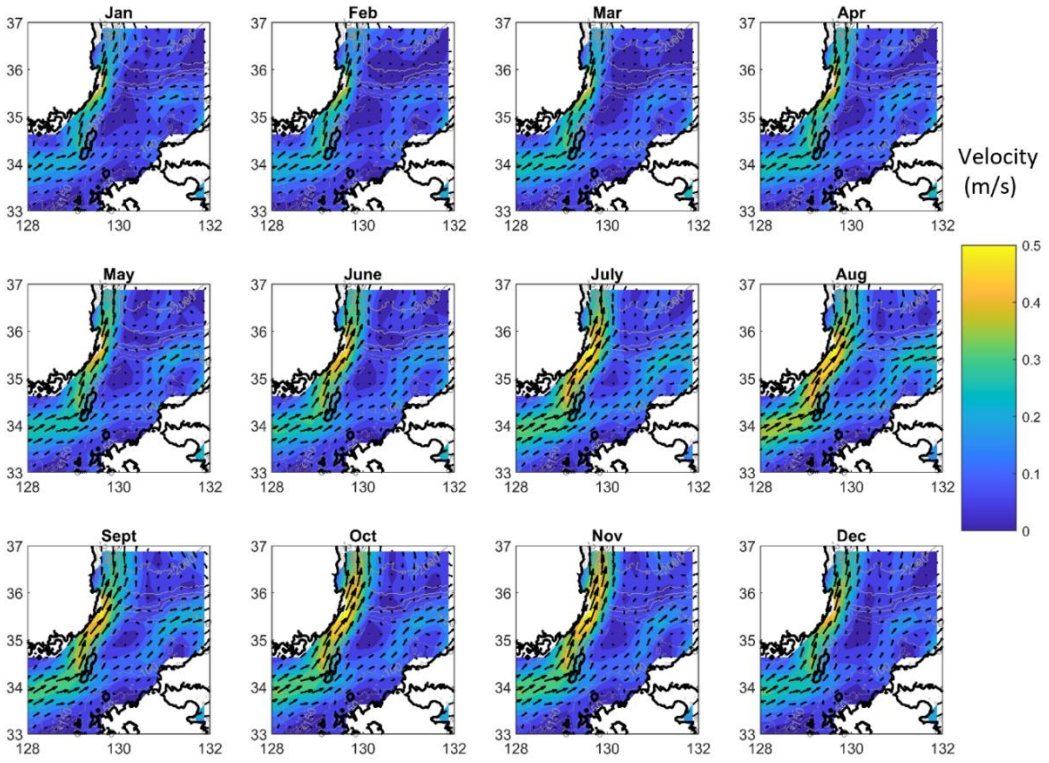

Figure 11. Monthly averages of surface velocity (m/s) calculated using 24 years of geostrophic velocities from CMEMS satellite altimetry

5.1 Long-term averages of branch transport

Here, we utilize 24 years of the CMEMS geostrophic current dataset to make volume transport estimates of the TWC and its subsequent branches. Although there have been estimates of KTS transport made using altimetry, such as Yabe et al. (2021), none have focused specifically on constraining the transport made by the along-shelf branch of the TWC. Transport estimates using bottom mounted, ship mounted, and moored current meters with durations of several months or longer have been available since the 1990s (Isobe et al., 1994, Isobe et al., 2002; Katoh et al., 1996; Teague et al., 2002). More recently, the ferry based ADCP measurements, such as those reported in Takikawa et al. (2005) and in Fukudome et al. (2010), have provided longer temporal coverage for volume transport estimates in the KTS. To better compare our estimates of transport with those in literature, we have chosen to include transport sections that are consistent with the ferry transects.

Transect	Endpoint 1 Latitude, Longitude	Endpoint 2 Latitude, Longitude
FB-S	35.09,129.10	34.73, 129.54
Shelf-N	35.6 130.4	36.5 130.4
Shelf-S	35.0, 130.4	35.6, 130.4
Near Shore	35.0 130.4	34.3 130.9

Table 2. locations used to determine current transport estimates.

For the purpose of this report, we define the following volume transport segments the endpoints of which are reported in table 2 and illustrated in Figure 12. The ferry boat path travelling between Busan, Korea and Hakata, Japan is split into a northwestern segment and southeastern segment, with the split occurring where the ferry rout turns past Tsushima Island. The total time-varying transports across each section is the integral over the cross-sectional area of the interpolated velocity normal to each section shown in Figure 12, and can be defined as:

$$Transport(t) = \int_0^L \int_{-Z}^0 V(t,l,z)\, dL\, dz \qquad (3)$$

where *V* is the velocity normal to each section, and *L* and *Z* are the length and depth of each section respectively. Because remote sensed geostrophic velocities are constrained to the surface, we estimate our transport assuming uniform velocities to a depth of 100m. The choice of this depth was in part informed by the shallowest depths across the KTS, and in part by the

average depth observed in the upper layer at mooring site A3. Following these approximations, we calculate an estimated transport for each section as follows:

$$Transport(t) \approx L * V * 100\, m \qquad (4)$$

Results of our transport estimates for four sections are shown in Figure 13. We begin by first comparing the results to historic data. For the comparisons presented in this work, we treat the KTS transport as the sum of both the northern and southern sections (FB-N+ FB-S). The along-shelf branch transport is also presented as a sum of both the northern and southern sections (Shelf-N+ Shelf-S) shown for simplicity. During certain time periods, we are able to compare our estimates with other historic measurements. The monthly averaged ADCP based estimates from the ferryboat *Camellia* are shown between 1997 and 2007 (Fukudome et al. 2010) are show with a thin dashed black line, and estimates made using bottom mounted ADCPs between May 1999 and March 2000 (Teague et al., 2002) are shown with black circles.

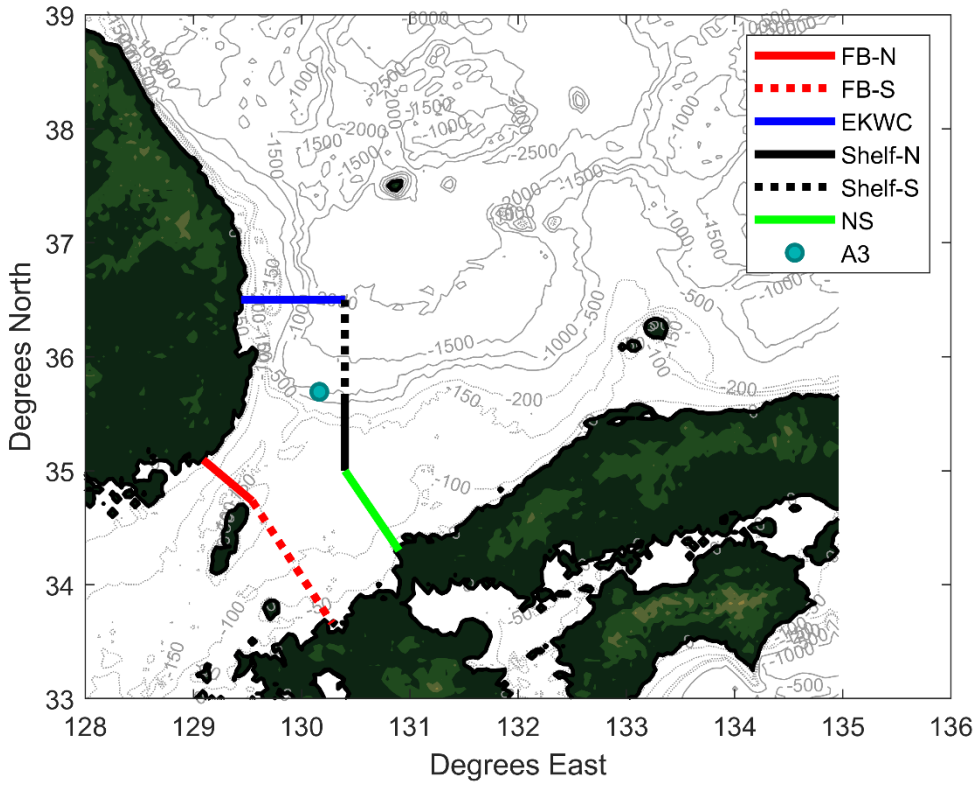

Figure 12. Map of JES showing where transport sections are calculated.

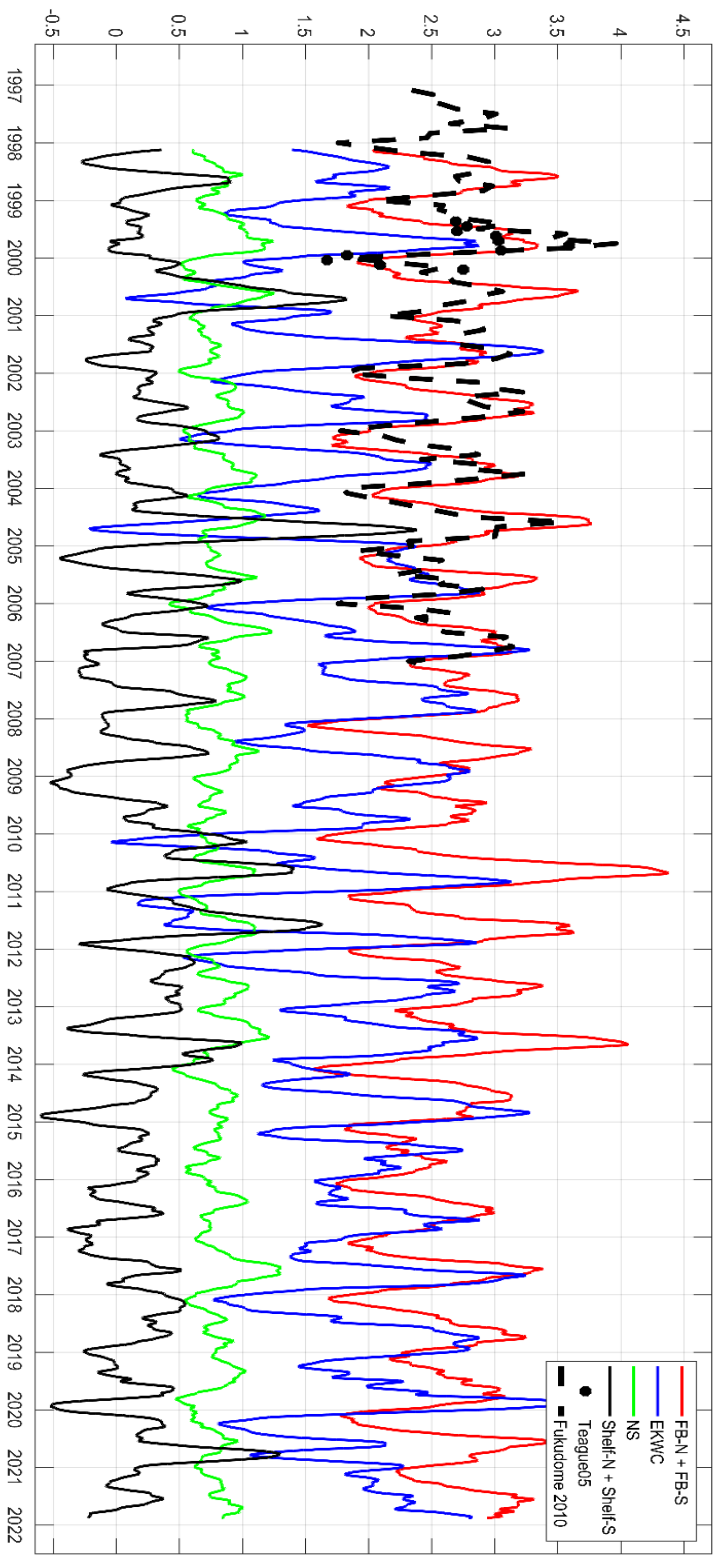

Figure 13. Low-passed (60 day) transport estimates for the transport sections between 1998 and 2022. Comparisons to key historical datasets are included.

While there are some differences in instantaneous transport magnitudes, these estimates generally compare well with our CMEMs based estimates. Takikawa et al. (2005) showed that the annual mean volume transport of the TWC through the KTS was 2.64 Sv (1 Sv = 10^6 m^3 s^{-1}), and Teague et al., (2002) found a similar value of 2.7 Sv. Over 24 years of CMEMS data, we found the annually averaged KTS transport to be 2.66 Sv, lending confidence to our estimation methods. Over the same 24 years, the annually averaged transport for the EKWC line was 1.79 Sv, and the near shore branch was 1.04 Sv, while the along-shelf branch accounted for 0.45 Sv. Although the along-shelf transport is considerably smaller than other TWC branches, it still accounts for 10-15% of the total transport coming through the KTS.

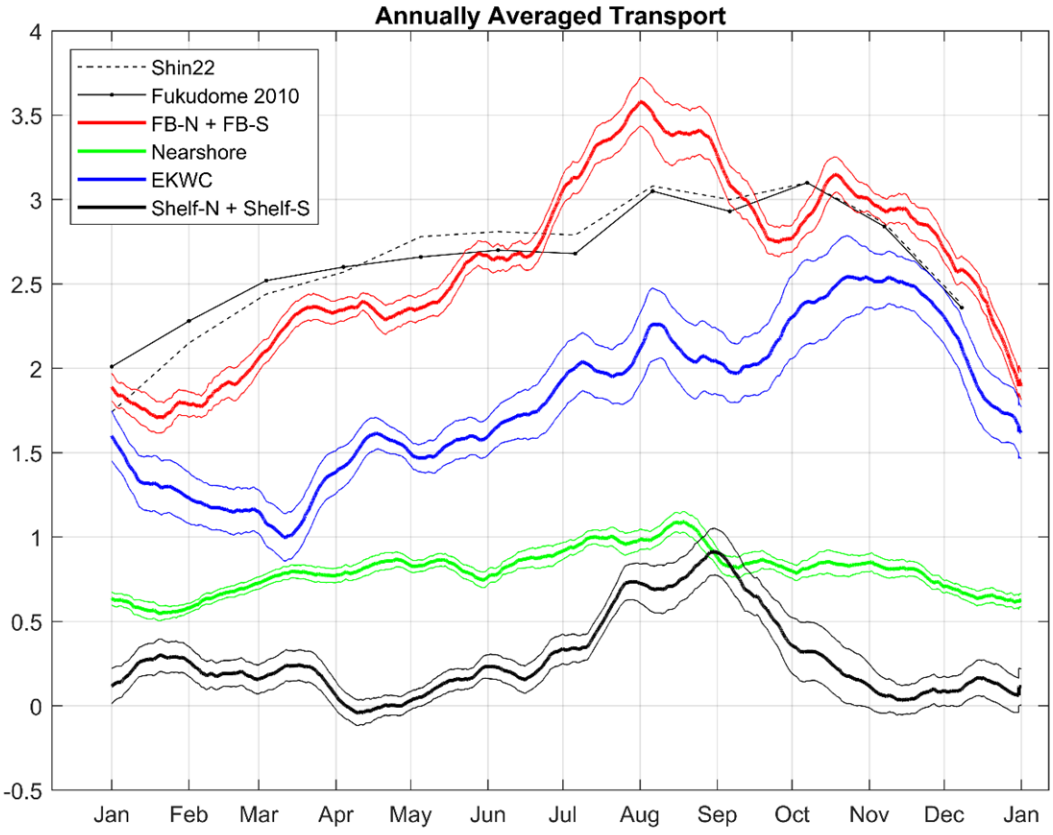

Figure 14. Monthly averages over all 24 years of CMEMS transport estimates 95th percentile confidence intervals are shown by thin lines.

When averaged monthly over all 24 years (Figure 14), the transport of the along-shelf branch peaks just below 1 Sv between August and September. All TWC branches examined had similar annual cycle trends in that the maximum transport occurred in summer months, and the minimum transport occurred in winter. The seasonal signal in the total KTS transport shows maximum transport of about 3.5 Sv in August and minimum transport less than 2.0 Sv in January-February. These estimates agree within to those reported in Shinn et al. (2022) and

Fukudome et al. (2010). Similarly, the seasonal signal in the EKWC transport shows maximum transport of about 2.5 Sv in November and minimum transport less than 1 Sv in February-March. The Nearshore (NS) transport shows much less annual variability, with transports between 0.5 and 1Sv. At times, the along-shelf transport is very near zero, or even slightly negative, implying that the flow along the basin shelf break in this area is occasionally arrested, and that these events occur most often in spring and fall.

5.2 Branching variability

In order to examine the frequency content variability of each transport section, we present variance preserving frequency spectra of each section performed over the duration of 24 years (Figure 15). All sections contain a visible peak at the annual cycle, although the nearshore branch contains the least variance at these frequencies, while the EKWC contains the most. Both the transport through the KTS and within the EKWC have the highest proportionality of variance contained within the annual cycle, but the along-shelf branch contains a large peak at 2 cycles per year, and another peak at 4 cycles per year. We do not at present have an explanation for the periodicity of these peaks, and it remains to be determined if these are representative of higher harmonics of the annual cycle or another phenomenon.

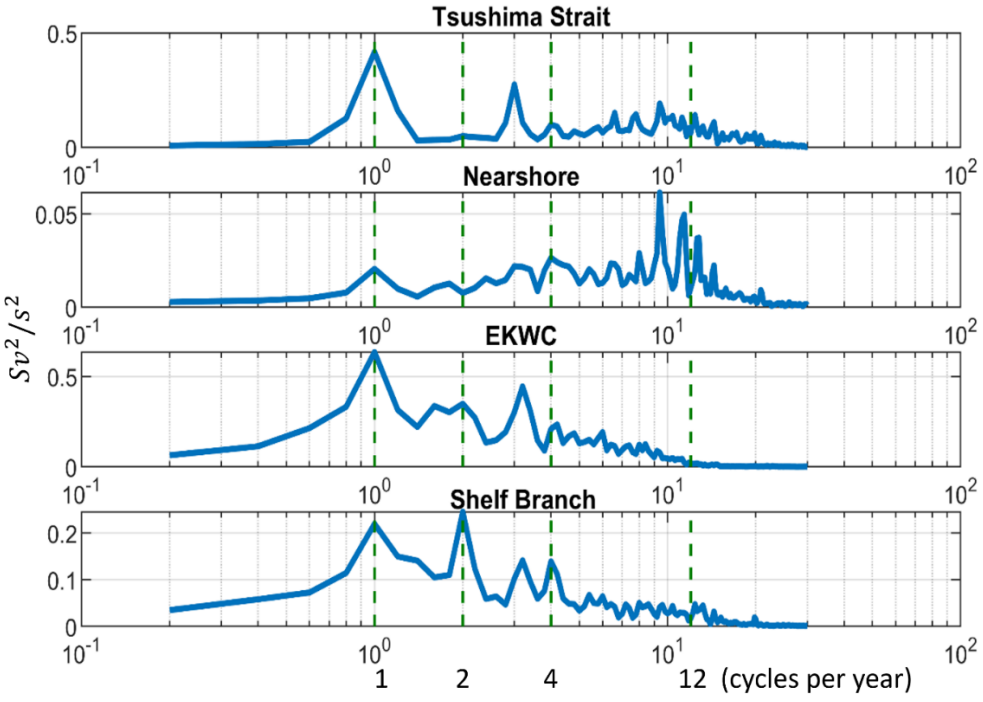

Figure 15. Variance preserving spectra of CMEMS derived transport estimates.

The total volume transport done by the nearshore branch was between 0.5 and 1.0 Sv, and it exhibits much less variability than through the KTS or other branches and did not appear

to show a strong yearly cycle, as was observed in the other branches. All branches contain some degree of higher frequency motions.

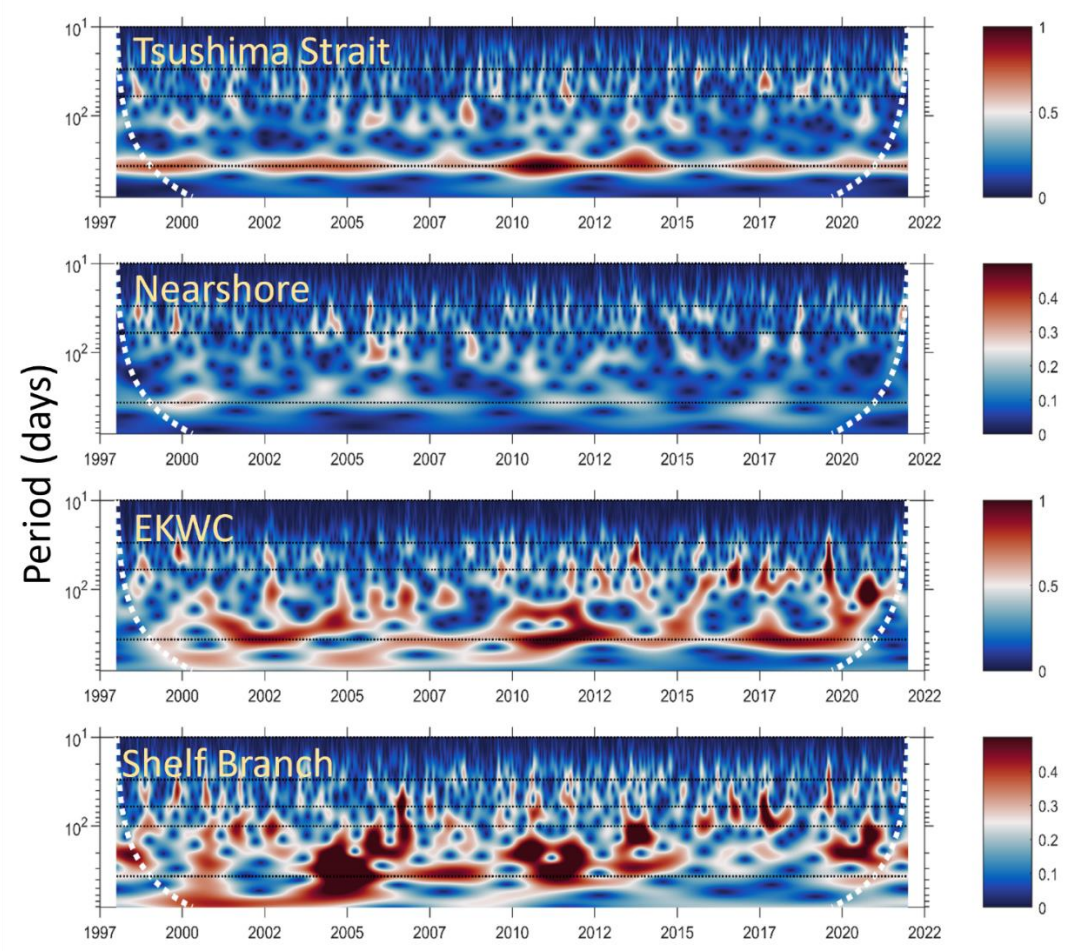

Figure 16. Wavelet transforms of each 24-year CMEMS transport time series. Horizontal lines are shown at periods of 30, 60, 100 days, and 1 year.

While Figure 13 highlights the low-frequency variability in our transport estimates, and Figure 15 illustrates the frequency content of each transport section, it is difficult to see the variability at periods less than a year, and how the transports on these timescales change from year to year. To show both the frequency content and the time variability inherent in our transport estimates, we utilize the continuous wavelet transform on each of the transport time-series to better characterize the signals. We use a generalized Morse wavelet which has a Fourier-domain form:

$$\Psi_{\beta,\gamma}(\omega) = \alpha_{\beta,\gamma}\omega^{\beta}e^{-\omega\gamma}, \qquad (5)$$

Where α is a normalization, and, $\gamma = 3$, $\beta = 7$, are chosen to optimize both the time and frequency resolution of the transform. Figure 16 presents the continuous wavelet transform

performed on each of the transport time-series. While similarities in transport variability exist among the different sections, notable distinctions also emerge. The nearshore branch accounts for a total volume transport ranging between 0.5 and 1.0 Sv. Notably, it demonstrates comparatively less variability than the transport through the KTS or other branches. Conversely, the along-shelf transport manifests a higher degree of sub-seasonal variability, particularly within the 30-60 day band, compared to the nearshore branch and the EKWC. Transport within the KTS primarily displays cyclic variability on annual time scales, indicating that the yearly cycle plays a dominant mode regulating variability. In contrast, both the EKWC and the along-shelf transport branch showcase more frequent periods of energetic transport occurring between one year and 100 days. Specifically, the EKWC transport exhibits episodic events within the 30 to 60 day range, occurring multiple times throughout the time-series. On the other hand, the along-shelf branch consistently demonstrates heightened variability within the 30 to 60 day range. This observation suggests that basin-scale eddy activity may play a significant role in regulating the along-shelf transport dynamics. The distinct variability patterns observed prompt further investigation into the potential influence of basin-scale eddy activity on the along-shelf transport, a topic which explore in the following section.

5.3 Dynamic Explanation for branching behavior

As has been suggested by Lee and Niiler 2010, one possible dynamic driver for the flow is conservation of potential vorticity, which exists as a balance in part between local relative vorticity and planetary vorticity. According to this theory, as the flow moves northward, it will experience an increasing Coriolis force, and therefore must loose (gain negative) relative vorticity in order to conserve potential vorticity. If the incoming flow already has sufficient negative relative vorticity, it may be able to overcome both the gain in planetary vorticity induced by its northward motion, as well as the vortex stretching term induced due to the sloping topography of the Ulleung basin. The net result is that the flow will turn right to conserve potential vorticity.

In order to explore the possible impact of upstream relative vorticity, we compute the vertical component of relative vorticity ζ/f using surface currents from the 24 years of remote data. Here, f is the Coriolis parameter, and the vertical component of relative vorticity is defined as:

$$\zeta = \frac{\partial v}{\partial x} - \frac{\partial u}{\partial y} \qquad (6)$$

where ∂u/∂y and ∂u/∂y are the horizontal shear of zonal and meridional current respectively. We examine the relative vorticity in the region, bin averaged over periods where the along-shelf transport was both high and low. We define low along-shelf branch transport to be less than -.05 Sv, and high along-shelf transport to be more than 1.0 Sv. Vorticity is then bin-averaged over these periods. The results of this averaging are shown in Figure 17. During both

periods of low and high along-shelf branch transport, the conditions upstream of the Tsushima Strait appear remarkably similar with respect to upstream, relative vorticity. In both cases, the averaged vorticity is positive along the coast of Korea upstream of Tsushima Island, and transitions to negative south of about 34°N. These similarities suggest that perhaps large-scale upstream vorticity does not play the leading role in determining the along-shelf branching behavior, as has been hypothesized.

One prominent difference in relative vorticity that can be seen in Figure 17 is the UWE at 36°N and 37.5°N, and between 130°E and 131°E, which appears as an area of negative relative vorticity during times of low along-shelf transport, indicating a warm eddy. To a lesser extent, but still somewhat visible in Figure 17 during the same time periods is an area of positive relative vorticity to the East of the UWE, which may be an indicator of the Dok Cold Eddy (DCE). The UWE and the DCE have been observed to persist for over a year and may offer an alternate explanation for the variability of the along-shelf transport. These eddies have also been found to influence the path of the EKWC in the southwestern JES (Lie et al., 1995). Mitchell et al. (2005) explained the eddy generation and nonlinear meandering of the EKWC using thin jet theory (Cushman-Roisin et al., 1993). It is possible that the variability of the EKWC and UWE control the strength of the along-shelf transport pathway. During times of expansion of the UWE, the EKWC meander neck becomes narrow until the DCE is pinched off from the meander. At the same time, this pushes the UWE south and westward, which effectively arrests the along-shelf transport. After these events, the UWE often moves northeastward, thus increasing transport in summer, which can be seen in Figure 17a. Future work to further constrain the dynamics that govern the along shelf flow could include evaluating the full three-dimensional potential vorticity budget within the southern JES, and diagnosing branching pathway strength as they relate to the generation of eddies through baroclinic instabilities.

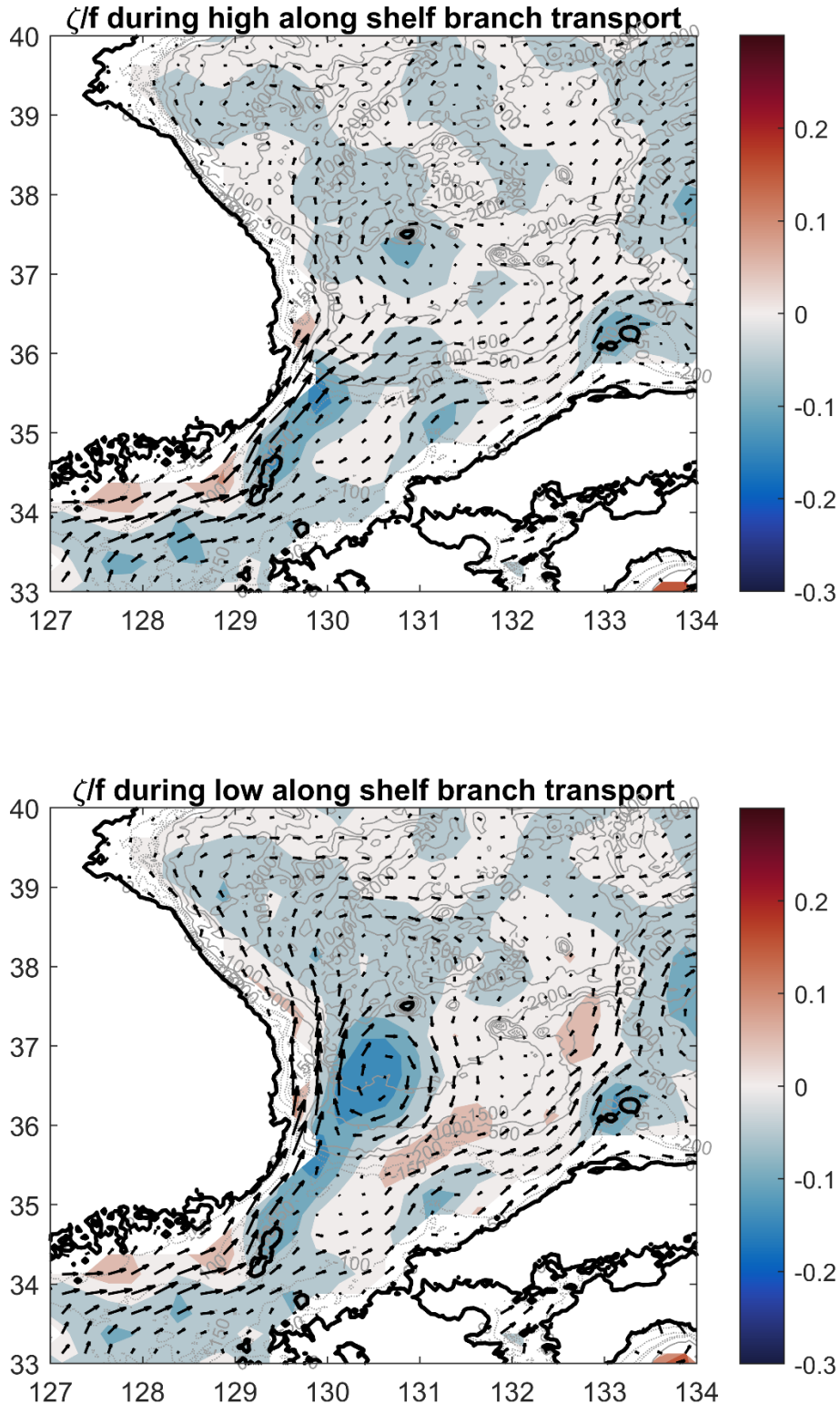

Figure 17. The vertical component of relative vorticity ζ/f computed using surface currents from the 24 years of CMEMS data.

6. Conclusions

Our investigation into the dynamics of a transport pathway in the East/Japan Sea (JES) and the Tsushima Warm Current (TWC) has revealed insights into the regional flow patterns and branching behavior. Our findings, including results from a drifter release, high-resolution ocean models, and examination of long-term satellite observations suggests that an along-shelf transport pathway exists intermittently, and contributes significantly to the regional transport. Furthermore, the results of this study show that this transport has both a clear seasonal cycle, and higher-frequency variability. By examining the regional vorticity derived from a remote sensing product, we present evidence that eddy forcing from within the JES, and interactions with the mean flow may be a leading factor in setting the TWC branching.

Our main inferences are as follows:

1) Drifter observations made during a 2021 field program in the JES show a distinct, along-shelf transport pathway. NRL models effectively recreate the observed drifter pathways. Higher model resolution corresponds with more realistic levels of horizontal drifter dispersion, and drifter trajectories closer to those seen in observations. Dispersion estimates revealed the influence of both local and nonlocal processes on spreading. The length scale at which the drifters transition to local diffusion processes implies that the local eddy field is important to regional transport dynamics and horizontal diffusivity. Moreover, synoptic scale weather events appear to be linked to high-frequency drifter motion.

2) The observed flow regime at the mooring site A3 was characterized by a two-layer system, with distinct dynamical features observed throughout the deployment period. Notably, flow reversals within the upper layer, occurring on timescales of 20-40 days, were indicative of the influence of Rossby waves and eddies. Comparisons of surface current observed at the A3 mooring with geostrophic currents derived from altimetry data suggest that while low-frequency surface currents generally aligned with altimetry-based estimates, significant departures exist at periods less than 30 days. Analysis of the wind-driven surface currents suggest but did not conclusively prove that wind driven flow may be important to these higher frequency motions.

3) An along-shelf transport pathway persists intermittently throughout the year, with a high degree of interannual variability. The timescales of this variability are supported by data from moored velocity records. Analysis of TWC branch transports using 24 years of geostrophic velocity data showcased the significance of the along-shelf transport, which contributed to approximately 16% of the total TWC transport. Furthermore, sub-seasonal variability, particularly within the 30-60 day range, was found to be more pronounced in the along-shelf transport compared to other branches.

4) An examination of relative vorticity suggests that that upstream vorticity conditions may not be a significant factor in determining TWS branching, and the existence of an along-shelf transport branch. While similarities were observed upstream of the Korea/Tsushima Strait during periods of both high and low along-shelf transport, the presence of warm and cold eddies introduced notable differences. These eddies, particularly the Ulleung Warm Eddy and the Dok Cold Eddy, may exert substantial influence on along-shelf transport variability. Their interaction with the East Korean Warm Current (EKWC) appears to play a crucial role in controlling strength of the along-shelf transport pathway.

The characteristics and dynamics of TWC branching and intermittent phenomenon such as the along-shelf transport pathway discussed here are difficult to study through observations, however by combining the in-situ data from a drifter release and observational field campaign with the remotely sensed data and the regional model output, we are able to make several key insights into the nature of a transport pathway in the JES. Our findings underscore the complex interplay between the TWC and eddies within the Ulleung Basin, which influence TWC branching variability. Our study offers valuable insights into branching behavior and local processes in the Southern Japan/East Sea, and identifies some possible directions for further research, such as a more thorough examination of potential vorticity budges, the spatio-temporal variability of potential vorticity, and the generation of baroclinic instabilities which lead to different TWC branching outcomes. Overall, our findings emphasize the importance of branching processes in the southern JES and underscore the need for a comprehensive understanding of the interactions between various factors which influence the regional dynamics.

7. Acknowledgments

This work was sponsored by the U.S. Navy through the NRL Karles Fellowship (grant 73-N21H-02-5), and as part of a collaborative effort between several South Korean institutions and the U.S. Naval Research Laboratory (NRL) project, “Mixing in the Japan/East Sea (MJES)”. Additionally, we thank NRL engineers Mr. Andrew Quaid and Mr. Ian Martens, as well as the many scientists, technicians, engineers and mariners on the R.V Onnuri who have been essential in the collection of the data presented here. The Author thanks NRL scientists Hemantha W. Wijesekera, Ewa Jarosz, David W. Wang, and Sergio Derada, Geosystem Research Corporation scientists Kyung-Il Chang and Jae Hak Lee, National Korea Institute of Ocean Science and Technology scientist Hong Sik Min, and Seoul National University scientist SungHyun Nam, for their collaboration in the work presented here. The model output, mooring data, and drifter tracks presented in this work are archived at NRL and available upon request from the author.

8. References

Book, J. W., Pistek, P., Perkins, H., Thompson, K. R., Teague, W. J., Jacobs, G. A., et al. (2004). Data assimilation modeling of the barotropic tides in the Korea/Tsushima Strait. *Journal of Oceanography, 60*, 977–993.

Chassignet, E. P., Hurlburt, H. E., Metzger, E. J., Smedstad, O. M., Cummings, J. A., Halliwell, G. R., ... Lozano, C. (2009). US GODAE Global Ocean Prediction with the HYbrid Coordinate Ocean Model (HYCOM). *Oceanography, 22*, 64–75.

Cho, Y., & Kim, K. (2000). Branching Mechanism of the Tsushima Current in the Korea Strait. *Journal of Physical Oceanography, 30*, 2788–2797. https://doi.org/10.1175/1520-0485(2000)030<2788:BMOTTC>2.0.CO;2

Cushman-Roisin, B., Pratt, L., & Ralph, E. (1993). A General Theory for Equivalent Barotropic Thin Jets. *Journal of Physical Oceanography*, *23*(1), 91-103. https://doi.org/10.1175/1520-0485(1993)023<0091:AGTFEB>2.0.CO;2

Drinkwater, K. F., & Loder, J. W. (2001). Near-surface horizontal convergence and dispersion near the tidal-mixing front on Northeastern Georges Bank. *Deep Sea Research Part II: Topical Studies in Oceanography, 48*(1–3), 311–339.

Fukudome, K. I., Yoon, J. H., Ostrovskii, A., et al. (2010). Seasonal volume transport variation in the Tsushima Warm Current through the Tsushima Straits from 10 years of ADCP observations. *Journal of Oceanography, 66*, 539–551. https://doi.org/10.1007/s10872-010-0045-5

Hase, H., Yoon, J.-H., & Koterayama, W. (1999). The current structure of the Tsushima Warm Current along the Japanese coast. *Journal of Oceanography, 55*, 217–235.

Hirose, N., & Ostrovski, A. G. (1999). Quasi-biennial variability in the Japan Sea. *Journal of Geophysical Research, 105*, 14011–14027.

Hogan, T. F., Rosmond, T. E., & National Centers for Environmental Prediction (U.S.). (2014). The description of the NMC spectral model (No. 468). U.S. Department of Commerce, National Oceanic and Atmospheric Administration, National Weather Service, National Centers for Environmental Prediction, Environmental Modeling Center.

Isobe, A., Ando, M., Watanabe, T., Senjyu, T., Sugihara, S., & Manda, A. (2002). Freshwater and temperature transports through the Tsushima–Korea Straits. *Journal of Geophysical Research, 107*(C7), 3065.

Isobe, A., S. Tawara, A. Kaneko and M. Kawano (1994): Seasonal variability in the Tsushima Warm Current, Tsushima-Korea Strait. *Cont. Shelf Res.*, **14**, 23–35.

Isoda, Y. (1994). Warm eddy movements in the eastern Japan Sea. *Journal of Oceanography, 50*, 1–15. https://doi.org/10.1007/BF02233852

Ito, M., Morimoto, A., Watanabe, T., Katoh, O., & Takikawa, T. (2014). Tsushima Warm Current paths in the southwestern part of the Japan Sea. *Progress in Oceanography, 121,* 83–93. https://doi.org/10.1016/j.pocean.2013.10.007

Itsuka Yabe, Yusuke Kawaguchi, Taku Wagawa, Shinzou Fujio. (2021). Anatomical study of Tsushima Warm Current system: Determination of Principal Pathways and its Variation. *Progress in Oceanography, 194*, 102590. https://doi.org/10.1016/j.pocean.2021.102590

Kantha, L. H., & Clayson, C. A. (2004). *Small-scale Processes in Geophysical Fluid Flows, Vol. 67.* Elsevier.

Katoh, S., Yasuda, I., & Watanabe, T. (1996). A Numerical Study of the Transition Region between the Kuroshio Extension and the Subarctic Front. *Journal of Physical Oceanography, 26*(2), 170–188. https://doi.org/10.1175/1520-0485(1996)026<0170:ANSOTT>2.0.CO;2

Kawabe, M. (1982). Branching of the Tsushima Current in the Japan Sea. *Journal of the Oceanographical Society of Japan, 38*, 183–192. https://doi.org/10.1007/BF02111101

Large, W. G., McWilliams, J. C., & Doney, S. C. (1994). Oceanic vertical mixing: A review and a model with a nonlocal boundary layer parameterization. *Reviews of Geophysics, 32*(4), 363–403. https://doi.org/10.1029/94RG01872

Lee, D.-K., & Niiler, P. (2010). Surface circulation in the southwestern Japan/East Sea as observed from drifters and sea surface height. *Deep Sea Research Part I: Oceanographic Research Papers, 57*(10), 1222–1232. https://doi.org/10.1016/j.dsr.2010.06.003

Lie, H. J. (1984). A note on water masses and general circulation in the Yellow Sea (Hwanghae). *한국해양학회지, 19*(2), 187–194.

Lilly, J. M. (2021), jLab: A data analysis package for Matlab, v.1.7.1, doi:10.5281/zenodo.4547006, http://www.jmlilly.net/software.

Luecke, C. A., Arbic, B. K., Bassette, S. L., Richman, J. G., Shriver, J. F., Alford, M. H., ... Wallcraft, A. J. (2017). The global mesoscale eddy available potential energy field in models and observations. *Journal of Geophysical Research: Oceans, 122*, 9126–9143. https://doi.org/10.1002/2017JC013136

Mellor, G. L., & Yamada, T. (1982). Development of a turbulence closure model for geophysical fluid problems. *Reviews of Geophysics and Space Physics, 20*(4), 851–875. https://doi.org/10.1029/RG020i004p00851

Moon, J.-H., Jang, H., Kim, T., Cha, H., & Hirose, N. (2023). Non-linear long-term trend in volume transport through the Korea/Tsushima Strait. *Frontiers in Marine Science, 10*, 1250452. https://doi.org/10.3389/fmars.2023.1250452

Morimoto, A., & Yanagi, T. (2001). Variability of Sea Surface Circulation in the Japan Sea. *Journal of Oceanography, 57*, 1–13. https://doi.org/10.1023/A:1011149401735

Oh, I. S., Zhurbas, V., & Park, W. (2000). Estimating horizontal diffusivity in the East Sea (Sea of Japan) and the northwest Pacific from satellite-tracked drifter data. *Journal of Geophysical Research, 105*(C3), 6483–6492. https://doi.org/10.1029/2000JC900002

Pak, G., Kim, Y. H., & Park, Y. G. (2019). Lagrangian approach for a new separation index of the East Korea Warm Current. *Ocean Science Journal, 54*, 29–38.

Preller, R. H., & Hogan, P. J. (1998). Oceanography of the Sea of Okhotsk and the Japan/East Sea. In A. R. Robinson & K. H. Brink (Eds.), *The Sea, vol. 11: The Global Coastal Ocean, Regional Studies and Synthesis* (pp. 429–481). Wiley.

Shin, H. R., Lee, J. H., Kim, C. H., Yoon, J. H., Hirose, N., Takikawa, T., & Cho, K. (2022). Long-term variation in volume transport of the Tsushima warm current estimated from ADCP current measurement and sea level differences in the Korea/Tsushima Strait. *Journal of Marine Systems, 232*, 103750.

SUDA, K. and K. HIDAKA (1932): The results of the oceanographical observations on board R. M. S. 'S yunpu Maru' in the southern part of the Japan Sea in the summer of 1929, part 1. J. *Oceanogr. Imp. Mar. Observ*., 3, 291-375 (in Japanese).

Takikawa, T., Yoon, J.-H., & Cho, K.-D. (2005). The Tsushima Warm Current through Tsushima Straits estimated from Ferryboat ADCP data. *Journal of Physical Oceanography, 35*, 1154–1168.

Teague, W. J., Jacobs, G. A., Perkins, H. T., & Book, J. W. (2002). Low-frequency current observations in the Korea-Tsushima Strait. *Journal of Physical Oceanography*, 32, 1621–1641.

Teague, W. J., Ko, D. S., Jacobs, G. A., Perkins, H. T., Book, J. W., Smith, S. R., ... Tang, T. Y. (2006). Currents through the Korea/Tsushima Strait: A review of LINKS observations. Oceanography, 19(3), 50–63. https://doi.org/10.5670/oceanog.2006.43

Toba, Y., Kawamura, H., Yamashita, F., & Hanawa, K. (1984). Structure of horizontal turbulence in the Japan Sea. In T. Ichiye (Ed.), *Ocean Hydrodynamics of the Japan and East China Seas* (pp. 317–332). Elsevier Oceanography Series, 39.

Torrence, C., & Compo, G. P. (1998). A Practical Guide to Wavelet Analysis. *Bulletin of the American Meteorological Society, 79*(1), 61–78. https://doi.org/10.1175/1520-0477(1998)079<0061:APGTWA>2.0.CO;2

Watanabe, T., Simizu, D., Nishiuchi, K., et al. (2009). Surface current structure of the Tsushima Warm Current region in the Japan Sea derived by satellite-tracked surface drifters. *Journal of Oceanography, 65*, 791–801. https://doi.org/10.1007/s10872-009-0066-0